Soil Dynamics and Earthquake Engineering 134 (2020) 106161

Contents lists available at ScienceDirect

Soil Dynamics and Earthquake Engineering

journal homepage: http://www.elsevier.com/locate/soildyn

An improved equivalent energy-based design procedure for seismic isolation system of simply supported bridge in China's high-speed railway

Wei Guo [a,b], Qiaodan Du [a,b], Zhe Huang [f], Hongye Gou [c,*], Xu Xie [d], Yong Li [e]

[a] School of Civil Engineering, Central South University, Changsha, 410075, China
[b] National Engineering Laboratory for High Speed Railway Construction, Changsha, 410075, China
[c] School of Civil Engineering, Southwest Jiaotong University, Chengdu, 610031, China
[d] Department of Civil Engineering, University of British Columbia, Vancouver, V6T 1Z4, Canada
[e] Department of Civil and Environmental Engineering, University of Alberta, Edmonton, T5J 4P6, Canada
[f] Changsha Pilot Investment Holdings Group Co.,Ltd, Changsha, 410006, China

ARTICLE INFO

Keywords:
High-speed railway bridge
Earthquake
Friction pendulum bearing (FPB)
Isolation
Energy-based design procedure (EEDP)
Seismic performance

ABSTRACT

The high-speed railway (HSR) in China has developed rapidly in recent years. However, HSR bridges have to face the challenge of earthquakes since China is one of the most earthquake-prone countries in the world. Bearing is the key component in the HSR bridge, and using isolation bearing instead of common bearing (non isolation bearing) can provide bridge the better seismic performance. To improve seismic performance of HSR bridges at different earthquake intensities, in this paper the friction pendulum bearing (FPB) is used, and an improved equivalent energy-based design procedure (EEDP) based on the principle of energy conservation is proposed. This method has the advantages of simple calculation and avoiding complicated iterations, which can also take into account the post-yield stiffness of the structural members and is capable of designing three performance objectives simultaneously. Meanwhile, based on the analysis of experimental data, the improved performance objectives applicable to the isolated HSR bridges are proposed. The FPB of an isolated HSR bridge is designed by the improved EEDP to verify the applicability of the proposed method. Then the finite element model of the designed isolated HSR bridge is built, and nonlinear dynamic responses at different earthquake intensities are analyzed to examine the structural seismic performance. Results show that the designed structure can achieve the prescribed performance objectives at three earthquake intensities which proves the practicability and effectiveness of the proposed improved EEDP method.

1. Introduction

The development of China's high-speed railway (HSR) has rapidly progressed in recent years, characterized with the total mileage of in-service railway lines exceeding 31,000 km in 2019. By the year of 2030, China's HSR network is expected to cover most areas of China with eight longitudinal lines in the south-north direction and eight transverse lines in the west-east direction respectively. Due to the necessity of protecting arable lands and the advantage of rapid construction, the majority of HSR lines generally consist of bridges [1], as shown in Fig. 1; for instance, in both the Beijing-Shanghai line and the Beijing-Guangzhou line, bridge portions comprise more than 80% of the lines' total mileage [2]. As China is one of the most earthquake-prone countries in the world, these bridges face the earthquake challenge and 80% of the line run through high seismic risk areas. Like the pipeline's distribution [3–5], the HSR line is also inevitable to avoid earthquake threat. Chinese earthquake records and railway lines are shown in Fig. 2. The Wenchuan earthquake of China in 2008 caused a large number of irreparable damages to bridges [6]. In addition, most of HSR bridges in China are simply supported bridges with common span of 32 m, and with much stronger girders and piers to ensure the line's smoothness for moving train [7,8]. There are several researches related with seismic analysis [9–12] and dynamic interaction of train and bridge coupled system of HSR bridges [13–16]. Theoretical researches and experimental tests validated that HSR bridges could resist common earthquakes, however, in extreme event bridge may collapse under strong earthquakes [17]. Reinforcement ratios of piers are required to be increased to improve the seismic performance of bridges, however,

* Corresponding author.
E-mail addresses: guowei@csu.edu.cn (W. Guo), 17877780807@163.com (Q. Du), 309811664@qq.com (Z. Huang), gouhongye@163.com (H. Gou), ryan20091101@gmail.com (X. Xie), yong9@ualberta.ca (Y. Li).

https://doi.org/10.1016/j.soildyn.2020.106161
Received 15 January 2020; Received in revised form 23 March 2020; Accepted 26 March 2020
Available online 13 April 2020

Fig. 1. Moving train on HSR bridges.

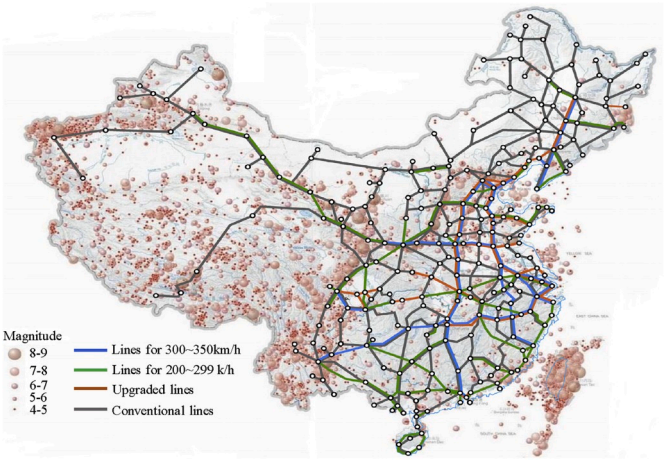

Fig. 2. Chinese earthquake records and railway lines.

which means more economic investments [18]. Compared with bridge piers, girders, and track structures, the bearings are relatively easily replaced, less expensive, and are the key components of bridge. Isolation techniques have been extensively used to improve the seismic performance of the bridge structures [19], considering the economic investments and seismic performance of HSR bridges under different earthquake intensities, it is a good choice to use the isolation bearing to reduce seismic damage and minimize the downtime of those HSR simply supported bridges.

To ensure a rapid repair and even immediate function recovery of HSR bridges after earthquakes, the protection of the HSR bridges against earthquakes is demanding, and the corresponding requirements of isolation bearing are much higher than other traditional ones. Several numerical and experimental studies show that the friction pendulum bearing (FPB) has great advantages, because of high bearing capacity, large displacement capacity, perfect durability, automatic restoration and variable natural vibration period controlled by the slide radius. Yu et al. [20] analyzed the effects of FPB on the responses of simply supported bridges of high-speed railway under longitudinal earthquakes, and the results show that FPB can effectively protect the bridge and track structures. Tsopelas et al. [21] conducted an experiment to compare the seismic responses of an isolated bridge with FPB and a non-isolated bridge, demonstrating a substantial improvement in the ability of the isolated bridge to sustain all levels of seismic excitation. Kim and Yun [22] studied a double concave friction pendulum system with various friction values and restoring properties on a bridge under various earthquake excitations. Morgan and Mahin [23] presented some numerical investigations to characterize the performance of a new multi-stage FPB, capable of progressively exhibiting different hysteretic properties at various levels of displacement demand. Fenz and Constantinou [24] described the principles of operation of the double concave FPB and presents the development of the force displacement relationship based on considerations of equilibrium. Mosqueda et al. [25] examined the behavior of FPB under multiple components of excitation through experimental and numerical studies.

To ensure better performance of isolated HSR bridges under different earthquake intensities, rational performance objectives and design method should be taken into adequate account. At present, performance-based seismic design method is widely accepted, in which the design criteria are expressed in terms of achieving stated performance objectives when the structure is subjected to stated levels of seismic hazard [26]. Calvi et al. [27] discussed the objectives of an isolation system for a bridge structure and presented a displacement-based design approach using a linear equivalent single degree-of-freedom model. Jara and Casas [28] proposed an extension of the displacement-based design procedure for bridges supported on hysteretic isolation bearings. Gardone et al. [29] estimated the target displacement of the structure through the acceleration-displacement response spectrum, and proposed a method for seismic design of new bridges and strengthening of old bridges. Priestley et al. [30] proposed the direct displacement-based design (DDBD) method. Okuda et al. [31] carried out a seismic performance retrofit study against large-scale earthquakes on an existing bridge. Li and Conte [32] applied an advanced probabilistic performance-based optimum seismic design methodology to the isolation system for a California high-speed rail prototype bridge, but this approach is complex and impractical for engineering design purposes. Goel et al. [33,34] proposed a performance-based plastic design (PBPD) method, in which the

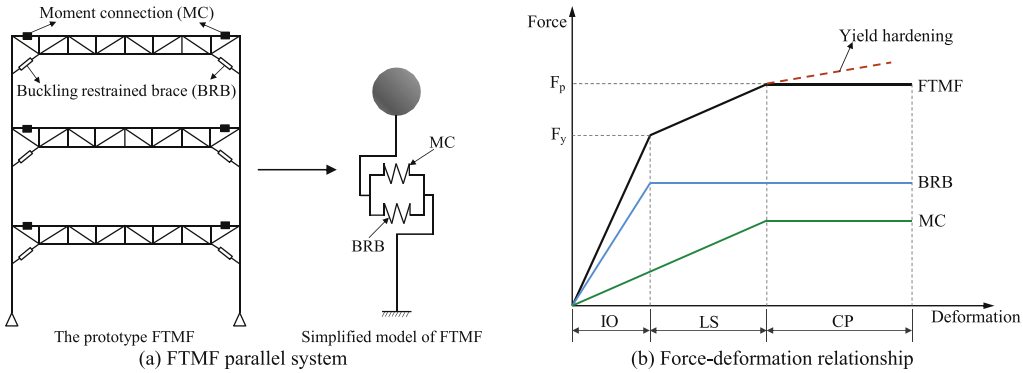

Fig. 3. FTMF parallel system and corresponding force-deformation relationship.

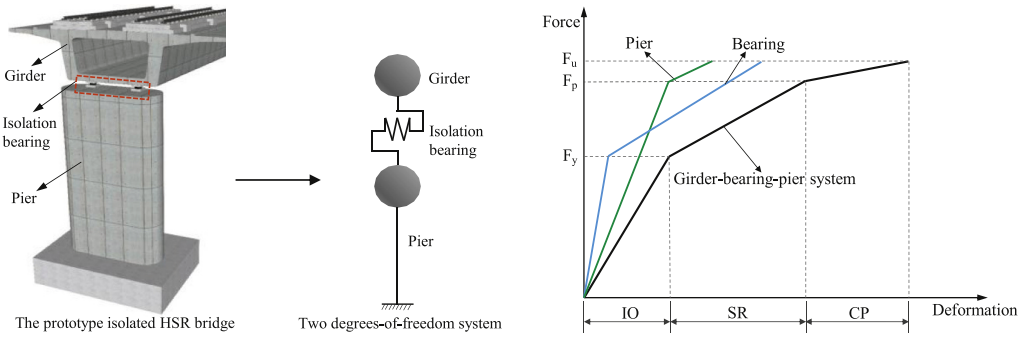

Fig. 4. Girder-bearing-pier series system and corresponding force-deformation relationship.

pre-selected target drift and yield mechanisms as key performance criteria. The design method assumes that a system has a bilinear force-deformation relationship, however, the isolated HSR bridge has a trilinear force-deformation relationship. Yang and Tung [35,36] presented a novel equivalent energy-based design procedure (EEDP) based on the concept of energy conservation and the response of an equivalent single degree of freedom (SDOF) for seismic resilient fused truss moment frame (FTMF) as shown in Fig. 3(a). A trilinear force-deformation relationship model is adopted in EEDP as shown by the black line in Fig. 3(b), which represents that EEDP can design three performance objectives. Furthermore, EEDP achieve the desired structural period, strength, and deformation with simple hand calculations without iterations. However, EEDP is currently mainly applied to parallel structures similar to FTMF as shown in Fig. 3(a), and the structural members designed by EEDP do not take into account post-yield stiffness as shown in Fig. 3(b). The girder-bearing-pier system of the isolated HSR bridge is actually a series structural system as shown in Fig. 4(a), so the previous EEDP method cannot be utilized. In addition, the post-yield stiffness of pier and bearing which are shown in Fig. 4(b) are also not considered in the previous EEDP method.

In this paper, FPB is adopted in HSR bridges to improve seismic performance under different earthquake intensities. However, the performance objectives in China's current code for seismic design of railway engineering are not applicable to the isolated HSR bridges. As such, the improved performance objectives applicable to the isolated HSR bridges are proposed, which are based on the analysis of existing experimental data. Furthermore, an improved EEDP method is proposed for the isolated HSR girder-bearing-pier series system. This method can take into account the post-yield stiffness of the structural members and is capable of designing three performance objectives simultaneously. To ensure the line's smoothness for moving train and improve the seismic performance of HSR bridge, a FPB of the isolated HSR bridge is designed by the improved EEDP method without changing pier and girder. To validate the effectiveness of the proposed EEDP method, finite element model of the isolated HSR bridge is built, and then nonlinear time history analyses are conducted for verification.

2. Seismic performance objectives of HSR bridge

Currently China's code for seismic design of railway engineering (GB50111-2006) [37] stipulates three-level performance objectives for HSR bridges. The determination of three performance objectives is related to the earthquake intensities. During the service level earthquake (SLE) with exceedance probability of 63.2% in 50 years, the performance is targeted to be immediate operation (IO), that means the HSR bridge is expected to be elastic, barely damaged and can guarantee the normal operation function after an earthquake. While subjected to the design based earthquake (DBE) with exceedance probability of 10% in 50 years, the performance is targeted to be short-term recovery (SR), and the HSR bridge system is expected to be repairable damaged and

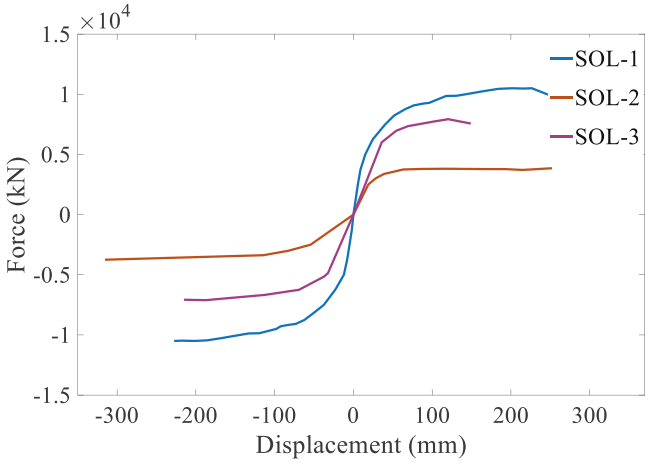

Fig. 5. The prototype's skeleton curve of the pier specimens.

present elastoplastic state. After an earthquake, the full functionality of bridge can be recovered in a short time. In the maximum considered earthquake (MCE) with exceedance probability of 2% in 50 years, the performance is designed to be collapse prevention (CP), that means the severe damage is allowed but the bridge does not collapse. Note that in the aforementioned performance objectives, although the overall performance state of the bridge structure is provided, the performance state of each member is unclear. More importantly, these performance objectives are applicable to the common seismic HSR bridges, not to the

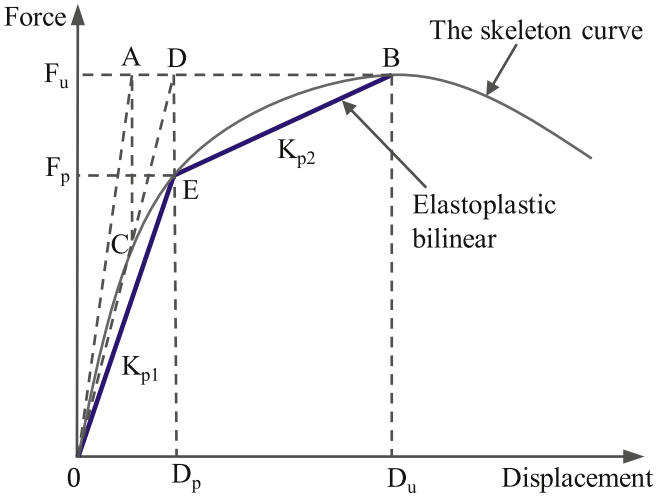

Fig. 6. Elastoplastic bilinear model of the pier.

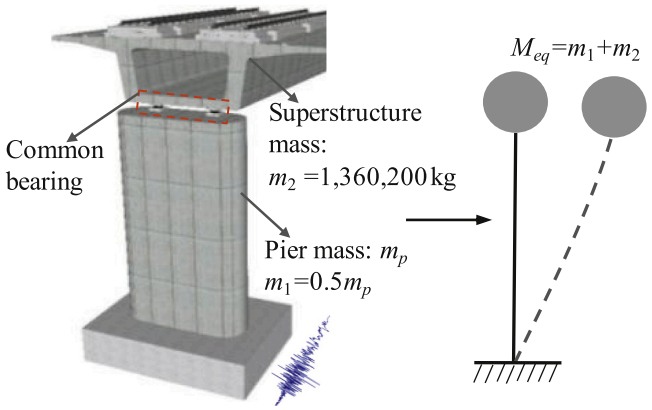

Fig. 7. The SDOF model of common HSR simply supported bridge.

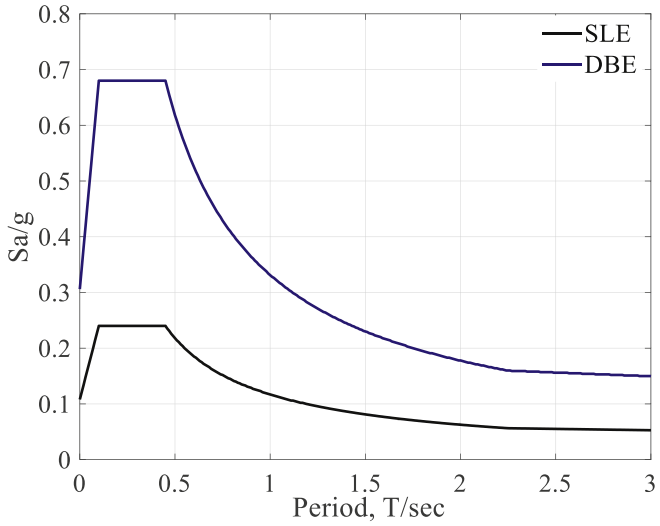

Fig. 8. Design response spectra.

isolated HSR bridges. Therefore, the improved performance objectives applicable to the isolated HSR bridges should be proposed.

2.1. Analysis of existing experimental data

Shao et al. [18] conducted a large number of theoretical and experimental analyses on the seismic performance of HSR piers. The experimental data of three 8 m prototype piers with different longitudinal reinforcement ratios, different axial load ratio and different stirrup ratio are reanalyzed in this paper, and specimen numbers of the three prototype piers are SOL1, SOL2 and SOL3. The prototype's skeleton curve of the pier specimens as shown in Fig. 5, which represents the force-deformation relationship, was simplified into an elastoplastic bilinear model by the geometric graphic method [38], and the turning point of the bilinear model is defined as the yield-state performance point of the pier. As shown in Fig. 6, K_{p1} and K_{p2} represent the elastic stiffness and the post-yield stiffness of the pier respectively. F_p and F_u represent the yield and the ultimate lateral force capacity of the pier, respectively, while D_p and D_u are the corresponding displacements of the pier. For a HSR bridge with common bearings, the superstructure is usually simplified to a lumped mass m_2 at the top of pier, the pier mass m_1 takes into account 50% of the actual mass m_p of the pier, and the pile-soil effect is not considered in this paper. The single-degree-of-freedom (SDOF) model is generally suggested for the seismic analysis and design of common HSR simply supported bridge in Chinese code [37], M_{eq} is the equivalent mass of SDOF model, as shown in Fig. 7. The tested pier is used as the typical substructure for a 32.6 m simply supported bridge, and the site condition of the bridge is classification II. The characteristic period zone of ground motions is the 3rd type, and the seismic fortification intensity is 8°, which are all defined by Chinese code. Fig. 8 shows the design response spectra specified in Chinese code, where the peak ground acceleration (PGA) of the SLE and DBE are 0.1 g and 0.3 g respectively. Based on these, the equivalent seismic force on the pier in the SLE and DBE are calculated using the capacity spectrum method. The seismic force is then compared with the yield force of pier to determine the pier state under earthquake. As shown in Table 1, the piers remain elastic during in SLE but yield in the DBE.

2.2. Improved performance objectives for isolated HSR bridges

Piers of HSR bridges in China often have large volume and cross-section to achieve great stiffness such that structural deformations are limited to guarantee the line smoothness ensuring high-speed moving train's safety under normal operation conditions. However, these strong piers remain elastic during the SLE but yield during the DBE by analyzing the existing experimental data. Moreover, theoretical researches and experimental tests validated that such strong HSR bridges could resist common earthquakes, however, may collapse during extreme large earthquakes [17]. Reinforcement ratios of piers should be increased to improve the seismic performance of bridges, but which means more economic investments [18]. It will be of great significance if the piers can be protected to avoid premature damage during the DBE by substituting common bearings with isolation bearings. But these performance objectives of Chinese code are be not applicable to the isolated HSR bridges. Therefore, this paper gives the improved performance objectives applicable to the isolated HSR bridges with FPB.

Fig. 9 shows the structure, isolation principle and hysteresis curve of FPB. Before sliding, FPB can provide enough shear force and stiffness to ensure the line smoothness and high-speed moving train's safety, and the shear pins restrict the relative motion between the upper and lower support plates of FPB. However, the earthquake will cut off those shear keys to cause FPB to slide like the bilateral sliding bearings. This sliding motion will isolate seismic forces, and the friction force will dissipate earthquake energy. So FPB is very suitable for HSR bridges. The FPB isolation principle is shown in Fig. 9 (b). When the girder relatively moves on the piers, the bearing between them vibrate like a pendulum with a certain period. The period can be changed to an expected value by adjusting the curvature radius R of pendulum [20]. By well designing FPB, HSR bridge can achieve different performance.

A well-designed isolated HSR bridge is able to achieve different

Table 1
Seismic design parameters for prototype of the pier specimen.

Specimen number	Pier mass m_p (kg)	Initial stiffness (kN/mm)	Yield force (kN)	Earthquake intensity	PGA (g)	Seismic force (kN)	Pier state
SOL-1	250,255	202.93	6407.18	SLE	0.1	3500.00	Not yield
				DBE	0.3	7852.23	Yielded
SOL-2	246,694	91.77	3266.47	SLE	0.1	2451.43	Not yield
				DBE	0.3	3749.86	Yielded
SOL-3	248,538	124.67	5525.92	SLE	0.1	2704.56	Not yield
				DBE	0.3	6902.36	Yielded

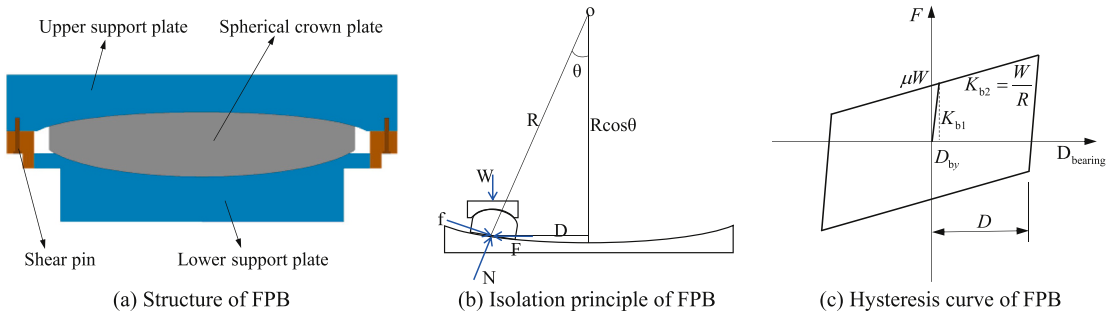

Fig. 9. Friction pendulum bearing (FPB).

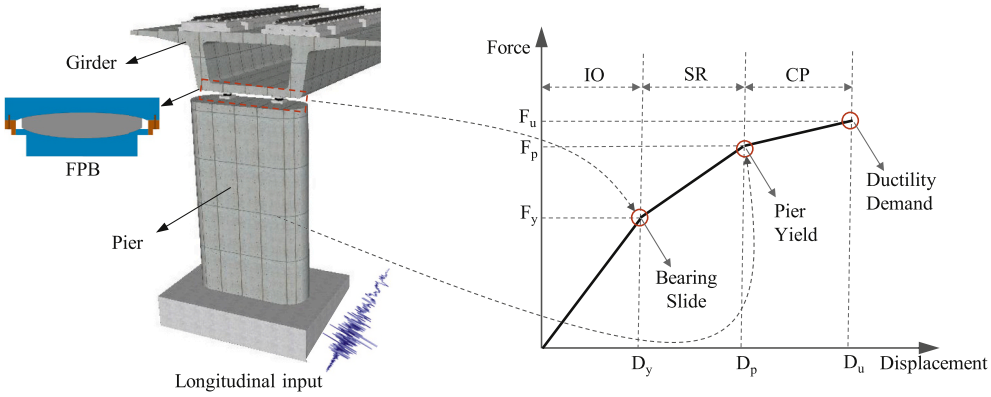

Fig. 10. Proposed performance objectives for isolated HSR bridges.

Table 2
Comparison of pier performance in common HSR bridge and isolated HSR bridge.

Earthquake intensity	Desired performance	Pier performance	
		Common HSR bridge	Isolated HSR bridge
SLE	IO	Elastic	Elastic
DBE	SR	Yield	Elastic
MCE	CP	Yield	Yield

performance objectives at different earthquake intensities. Based on analysis results and three performance objectives in Chinese code, the improved performance objectives also need to meet IO, SR and CP, and the desired force-deformation curve of the isolated HSR bridges is trilinear, as shown in Fig. 10. It is specifically described here: when an isolated HSR bridge is subjected to SLEs, all the bridge members remain elastic, in which the pier remains elastic and the bearing does not slide, corresponding to the first performance objective IO; when an isolated HSR bridge is subjected to DBEs, the pier remains elastic, the bearing starts to slide, and the sliding motion of bearing is used to isolate seismic forces and dissipate earthquake energy, corresponding to the second performance objective SR; when an isolated HSR bridge is subjected to MCEs, the pier yield and dissipate energy by hysteretic behavior, the pier's displacement ductility factor is required to be no larger than a value of 4.8 which is specified in Chinese code, and the bearing continues to slide to isolate seismic forces and dissipate earthquake energy, corresponding to the third performance objective CP. The pier is protected to avoid premature yielding during the DBE by substituting common bearings with isolation bearings. Table 2 compares the pier performance in common HSR bridge and isolated HSR bridge.

For the HSR FPB isolated bridge, if the friction coefficient μ for friction pendulum bearing under SLE excitation is well designed, the bearing does not slide, and the pier remains elastic for the performance objective of IO. If the earthquake intensity is greater than the SLE, the seismic force will be greater than F_{by} ($F_{by} = \mu W$, W is the weight of superstructure) of FPB, corresponding displacement is D_{by}, and the bearing will start to slide with the stiffness K_{b2} as shown in Fig. 11(a).

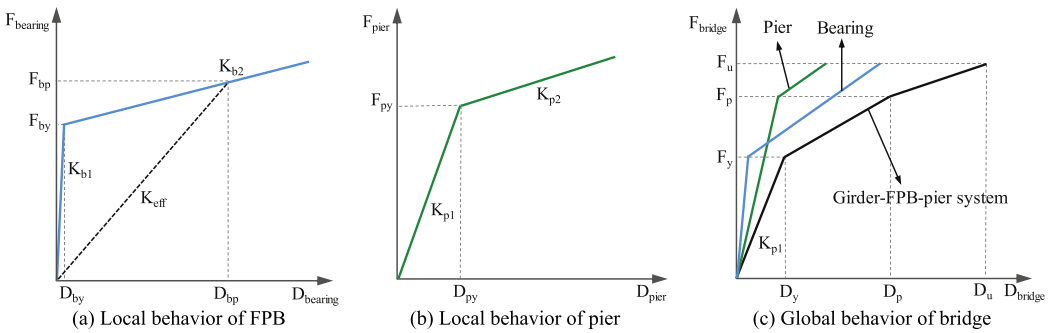

Fig. 11. Behavior of bearing, pier and isolated HSR bridge.

Under the excitation of DBE, by designing the sliding stiffness K_{b2} ($K_{b2} = W/R$, K_{b2} is designed by the size of the curvature radius R) of the friction pendulum bearing, the seismic force between the pier and girder can be adjusted, the pier remains elastic and the bearing starts to slide for the performance objective of SR. If the earthquake intensity is greater than the DBE, the seismic force will be greater than the yield base shear F_{py}, and the pier yields, as shown in Fig. 11(b). Under the excitation of MCE, the pier yield and the bearing continue to slide, and the pier ductility factor is checked for the performance objective of CP. The performance curve of isolated HSR bridge is illustrated in Fig. 11(c). It's obvious that the proposed performance objectives of isolated HSR bridge can be realized by designing the friction coefficient μ and the sliding stiffness coefficient K_{b2}.

3. Equivalent model of HSR simply supported bridge

In section 4, an improved EEDP method based on the concept of energy conservation will be proposed, and this method is based on the equivalent SDOF system. However, for the isolated HSR bridge to be designed, the isolation bearing and the pier are connected in series, and it can be simplified as a two-degree-of-freedom (TDOF) system. The series structural system of TDOF system needs to be equivalently transformed to be an equivalent nonlinear SDOF (ENLSDOF) system.

A common transformation in which a multi-degree-of-freedom (MDOF) system is equivalent to a SDOF system is introduced here. Firstly, assuming that the vector for the mode shape $\{\Phi\}$ of the MDOF system remains unchanged during the analysis, and the lateral displacement shape of the MDOF system is similar to the system's basic mode of vibration. The following equations are given based on the equivalent SDOF model:

$$\Gamma_1 * \Phi_{1s} = 1 \tag{1}$$

$$\Gamma_1 = \frac{\sum_{i=1}^{n} m_i \Phi_{1i}}{\sum_{i=1}^{n} m_i \Phi_{1i}^2} \tag{2}$$

where Γ_1 is the participation coefficient of the first mode, and Φ_{1s} is the mode vector value of the first mode shape of the equivalent SDOF system.

If both of SDOF and MDOF systems vibrate by the first mode, the maximum kinetic energy is assumed to be equal, and the following Equation (3) can be obtained:

$$\frac{1}{2} M_{eq} (\omega_1 x_m)^2 = \frac{1}{2} \sum_{i=1}^{n} m_i (\omega_1 x_i)^2 \tag{3}$$

where ω_1 is the circular vibration frequency of the first mode; M_{eq} and x_m are the mass and displacement of the equivalent SDOF model, respectively; and m_i and x_i are the mass and displacement of the ith node of the MDOF model respectively. Equation (4) can be derived from Equation (3) as follows:

$$M_{eq} = \frac{\sum_{i=1}^{n} m_i x_i^2}{x_m^2} \tag{4}$$

Because $x_i/x_m = \Phi_{1i}/\Phi_{1s}$ and $\Phi_{1s} = 1/\Gamma_1$, Equation (5) can be obtained as follows:

$$M_{eq} = \frac{\left(\sum_{i=1}^{n} m_i \Phi_{1i}\right)^2}{\sum_{i=1}^{n} m_i \Phi_{1i}^2} \tag{5}$$

For the HSR bridge isolated by FPB, it is simplified as a TDOF system. The relationship between the top displacement D of the TDOF system and the displacement d of the equivalent SDOF system is expressed in Equation (6):

$$D = d\Gamma_1 \Phi_{12} \tag{6}$$

where Φ_{12} is the mode vector value of the first mode shape at the top of TDOF system.

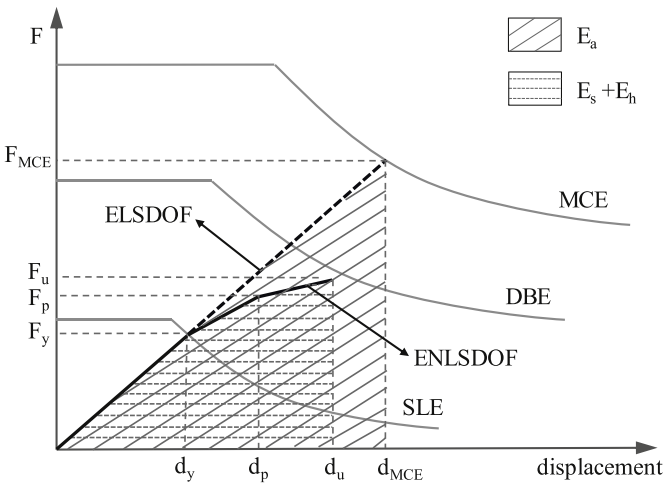

Fig. 12. Force-displacement relationship and energy conservation concept in improved EEDP.

4. The improved equivalent energy-based design procedure

The energy released by the earthquake is transmitted to the structure through the ground, causing the response of the structure. Therefore, there is a sufficient theoretical basis to balance the seismic demand and capacity of structure from the perspective of energy. Housner [39] proposed the energy-based seismic design concept at the first World Conference on Earthquake Engineering, and explained that the total energy E_i of a seismic input into the structure converts to different types of energy. While some of this energy is dissipated through damping E_ξ, the remaining energy is stored in the structure in the form of kinetic energy E_k, and strain energy E_a. If the structure were designed to remain elastic, E_a would be stored as elastic strain energy E_s. In the case where the structure yields, E_a will be divided into elastic strain, E_s, and hysteretic energy, E_h. Uang and Bertero [40] elaborated on this concept using the following Equation (7):

$$E_i = E_k + E_\xi + E_a = E_k + E_\xi + E_s + E_h \tag{7}$$

If a structure remains elastic under earthquake action, the strain energy to be stored in the equivalent linear SDOF (ELSDOF) model is transformed into elastic energy, which can be obtained through simple calculation. However, when a strong earthquake occurs, the structure will yield, and the strain energy of the ENLSDOF model will be dissipated through the vibration cycle. This portion of the energy needs to be obtained by a time history analysis of the structure. Yang and Tung [35, 36] proposed a novel EEDP based on the concept of energy conservation, which assumes that the energy input into the above two models are equal, and thus seismic energy of the ELSDOF model can calculated to obtain that of the ENLSDOF model. Furthermore, it's well known that when the ENLSDOF model is subjected to seismic excitation, the energy will be dissipated through all of the vibration cycles of model. For simplicity and convenient engineering application, a simple monotonic pushover process is adopted to equivalently describe the energy produced by seismic excitation. As the pushover process only corresponds to the monotonic maximum response of structure, the energy dissipated in the monotonic pushover process is less than that in the earthquake which is actually a cyclic process, and a modification factor larger than 1.0 is given for calculation of energy.

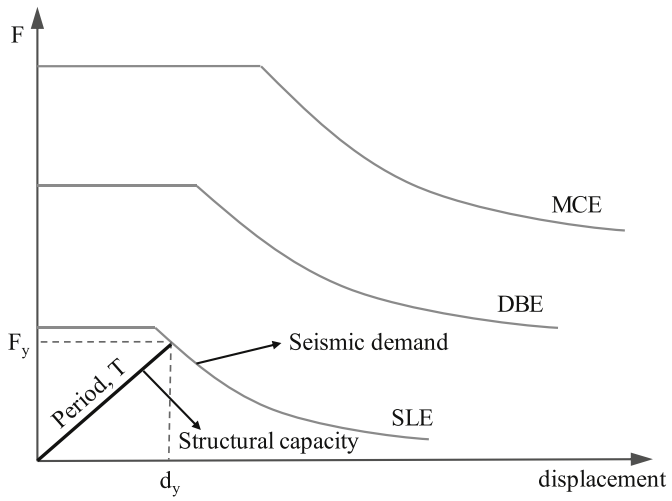

Fig. 13. Correlation of T, F_y, SLE, and d_y

Base on the above, an improved EEDP is proposed to be applied to the isolated HSR bridge in this paper, which also has the advantages of simple calculation and without complicated iterations, and considers the post-yield stiffness and displacement ductility of the structural members. Fig. 12 shows force-displacement relationship and energy conservation concept in improved EEDP. The force-deformation response of an isolated HSR bridge is approximated by the ENLSDOF system. The energy to be dissipated by the ENLSDOF system is equal to the energy of an ELSDOF system [35,36]. In Fig. 12, the vertical axis represents the base shear, which is calculated using the spectral acceleration, S_a, multiplied by the structural mass, m, and the horizontal axis represents the displacement of equivalent SDOF system. Through Equations (8) and (9), the response spectrum curve of the acceleration-period relationship at different earthquake intensity (SLE, DBE and MCE) can be transformed into the curve of the force-displacement relationship for the equivalent SDOF system in Fig. 12.

$$F = S_a \times m \tag{8}$$

$$d = S_a \frac{T^2}{4\pi^2} \tag{9}$$

where T is the period of the equivalent SDOF system.

4.1. IO performance objective at SLE

During the SLE intensity, the structure is designed to remain elastic for the performance objective of IO. As shown in Fig. 13, the force-deformation relationship shall remain linear. The balance point of structural capacity and seismic demand is determined by four parameters, namely the elastic period (T), yielding base shear (F_y), earthquake intensity at the SLE, and yielding displacement (d_y). Since these parameters are not independent, as long as two of the four parameters are determined, and the other two parameters can be obtained [35].

For the HSR bridge isolated by FPB, through the design of the friction coefficient μ for friction pendulum bearing, the FPB does not slide and the pier remains elastic for the performance objective of IO during the SLE intensity. At this time, the FPB initial stiffness K_{b1} is much greater than the pier stiffness K_{p1} and shear displacement D_{by} of FPB is less than 0.2 mm, so the FPB is similar to common fixed bearing and the deformation of the FPB is ignored. And the isolated HSR bridge is similar to a common HSR bridge, which can be directly simplified as a ELSDOF system with a mass of $M_{eq} = m_1 + m_2$ and an initial stiffness of the pier stiffness K_{p1}. Therefore, the fundamental period of the ELSDOF system is determined, as shown in Equation (10).

$$T = 2\pi\sqrt{\frac{M_{eq}}{K_{p1}}} \tag{10}$$

The SLE intensity is selected in GB50111-2006, with T determined, the yielding base shear F_y and yielding displacement d_y of the ELSDOF system can be identified from the intersection of the SLE curve and the ELSDOF capacity curve on Fig. 13. By distributing F_y to the pier and girder according to the mass ratio, the sliding force F_{by} of the FPB can be calculated, and the friction coefficient μ of the FPB is determined, as shown in Equations 11 and 12.

$$F_{by} = \frac{m_2}{m_1 + m_2} F_y \tag{11}$$

$$\mu = \frac{F_{by}}{W} = \frac{F_{by}}{m_2 \times g} \tag{12}$$

$$D_y = d_y = F_y / K_{p1} \tag{13}$$

where W is weight of superstructure, D_y is the top displacement of the isolated HSR bridge.

4.2. SR performance objective at DBE

When the isolated HSR bridge is subjected to the DBE intensity, the pier remains elastic, and the FPB starts to slide, corresponding to the second performance objective SR. The desired performances of the ELSDOF and ENLSDOF systems at DBE as shown in Fig. 14. The incremental energy of the ELSDOF system from the SLE to the DBE is defined as ΔE_{E1}, as determined by Equation (14). The incremental energy of the ENLSDOF model when subjected to ground motion from the SLE to the DBE is defined as ΔE_{ND1}, improved EEDP method equates the ΔE_{E1} to ΔE_{ND1} [35]. The incremental energy of the ENLSDOF model when pushed monotonically from the SLE to the DBE is defined as ΔE_{NM1}, which can be calculated by Equation (15). and ΔE_{ND1} and ΔE_{NM1} are connected by a modification factor γ_a. Equation (16) explains the relationship between the three types energy mentioned above. The energy

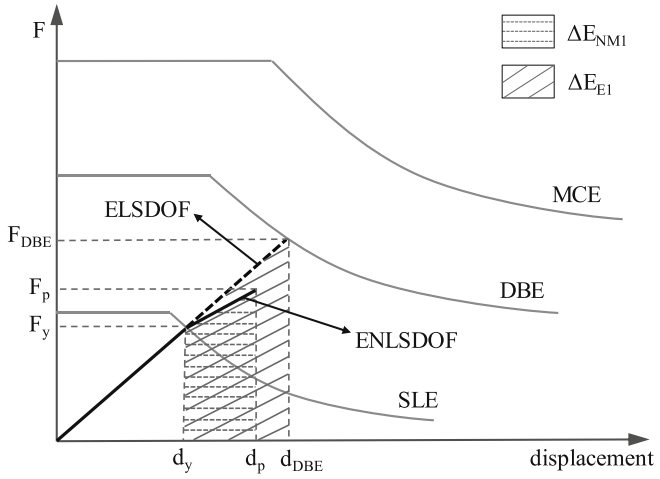

Fig. 14. The desired performances of the ELSDOF and ENLSDOF systems at DBE.

$$\Delta E_{E1} = \frac{1}{2}\left(F_y + F_{DBE}\right)\cdot\left(d_{DBE} - d_y\right) \tag{14}$$

$$\Delta E_{NM1} = \frac{1}{2}\left(F_p + F_y\right)\cdot\left(d_p - d_y\right) \tag{15}$$

$$\Delta E_{E1} = \Delta E_{ND1} = \gamma_a \Delta E_{NM1} \tag{16}$$

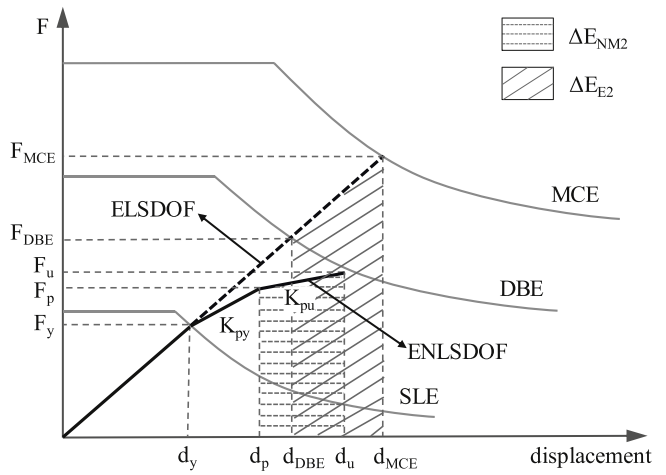

Fig. 15. The desired performances of the ELSDOF and ENLSDOF systems at MCE.

modification factor γ_a will be explained in section 4.5.

Substituting Equations (14) and (15) into Equation (16) gives the plastic displacement d_p of ENLSDOF system, as shown in Equation (17).

$$d_p = \frac{2\Delta E_{E1}}{\gamma_a (F_p + F_y)} + d_y \tag{17}$$

where F_{DBE} and d_{DBE} are base shear and displacement of the ELSDOF system at the DBE intensity, respectively, can be identified from the intersection of the DBE curve and the ELSDOF capacity curve on Fig. 14. F_p and d_p are base shear and displacement of the ENLSDOF system at DBE intensity respectively, it should be noted that F_p is equal to the yield base shear F_{py} of the pier. Assuming that the vibration of the isolated HSR bridge is mainly controlled by the first mode, and the secant stiffness K_{eff} corresponding displacement D_{bp} of the FPB at DBE intensity as shown in Fig. 11(a), is employed to perform the mode analysis together with the pier stiffness K_{p1}. After obtaining d_p, K_{eff} and D_{bp} can be obtained through Equations (2) and (6) from the section 3, and the sliding stiffness K_{b2} of the FPB can be calculated. Until now, IO performance objective at SLE intensity and SR performance objective at the DBE intensity are achieved by the design of the FPB.

4.3. CP performance objective at MCE

During the DBE intensity, the isolated HSR bridge need to withstand the earthquake attack without collapse, corresponding to the third performance objective CP. At this time, the pier yield and dissipate energy by hysteretic behavior, and the FPB continues to slide to isolate seismic forces and dissipate earthquake energy. The isolated HSR bridge creates a trilinear force-deformation response corresponding to the ENLSDOF system as shown in Fig. 15, in which K_{py} and K_{pu} are post-yield stiffness and post-yield ultimate stiffness of the ENLSDOF system, respectively. The performance objective CP is achieved by designing the FPB to limit the ultimate displacement of the pier, to ensure that the ductility factor of the pier is no larger than the value of 4.8.

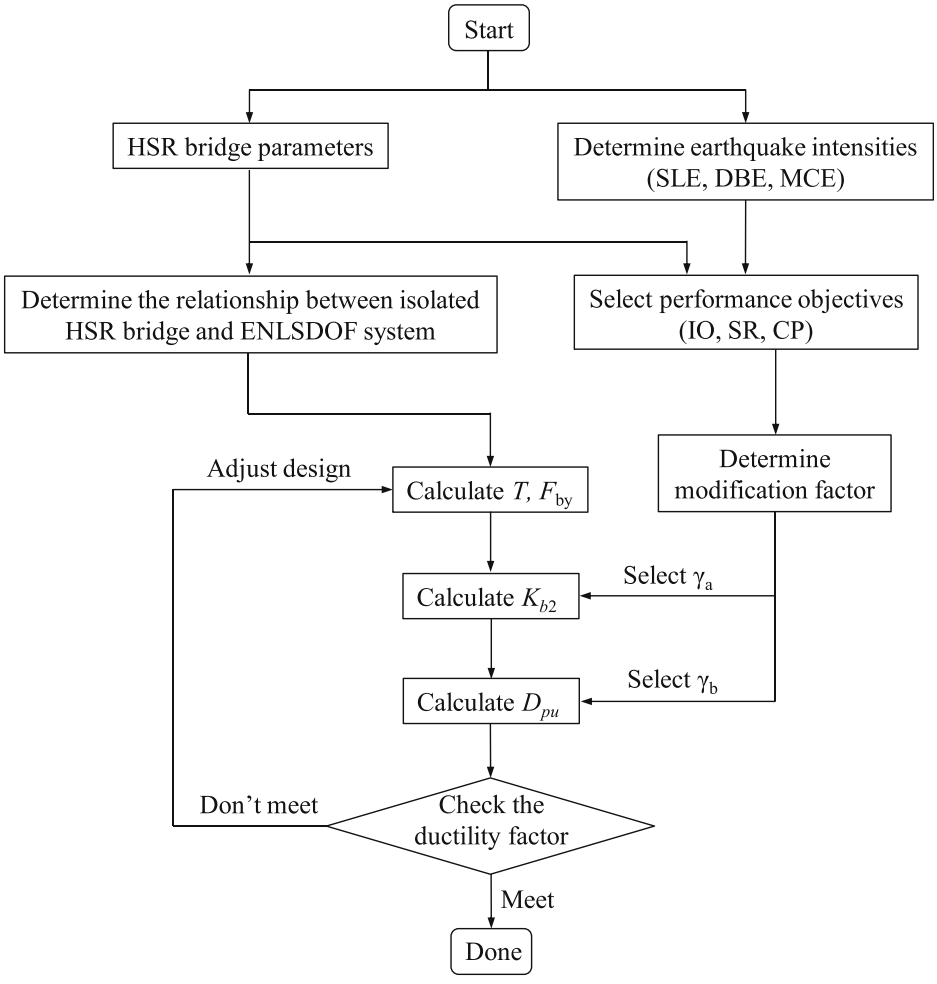

Fig. 16. Design flowchart of the improved EEDP method for isolated HSR bridge.

The incremental energy of the ELSDOF model from the DBE to the MCE is defined as ΔE_{E2}, which can be determined by Equation (18). The incremental energy of the ENLSDOF system when subjected to ground motion from the DBE to the MCE is defined as ΔE_{ND2}. The incremental energy of the ENLSDOF system when pushed monotonically from the DBE to the MCE is defined as ΔE_{NM2}, which can be determined by Equation (19). Improved EEDP equates the ΔE_{E2} to ΔE_{ND2} [35], and ΔE_{ND2} and ΔE_{NM2} are connected by a modification factor γ_b, Equation (20) explains the relationship between the three types energy mentioned above. Fig. 15 shows the relationship between ΔE_{E2} and ΔE_{NM2} and the desired performances of the ELSDOF and ENLSDOF systems at MCE. The energy modification factor γ_b is similar to γ_a, which will be introduced in section 4.6.

$$\Delta E_{E2} = \frac{1}{2}(F_{MCE} + F_{DBE}) \cdot (d_{MCE} - d_{DBE}) \tag{18}$$

$$\Delta E_{NM2} = \frac{1}{2}(F_u + F_p) \cdot (d_u - d_p) \tag{19}$$

$$\Delta E_{E2} = \Delta E_{ND2} = \gamma_b \Delta E_{NM2} \tag{20}$$

Substituting Equations (18) and (19) into Equation (20) gives the ultimate base shear F_u of ENLSDOF system, as shown in Equation (21).

$$F_u = \frac{2\Delta E_{E2}}{\gamma_b (d_u - d_p)} - F_p \tag{21}$$

where F_{MCE} and d_{MCE} are base shear and top displacement of the ELSDOF system at the MCE intensity, respectively, can be identified from the intersection of the MCE curve and the ELSDOF capacity curve on Fig. 15. F_u and d_u are base shear and top displacement of the ENLSDOF system at the MCE intensity, respectively. For the isolated HSR bridge, in Equation (21): $d_u - d_p = (F_u - F_p)/k_{pu}$, and $K_{pu} = k_{p2} \cdot k_{b2}/(k_{p2} + k_{b2})$. It is well known that F_u is equal to the ultimate base shear F_{pu} of pier, and thus the ultimate displacement D_{pu} of the pier at the MCE can be calculated by Equation (22).

$$D_{pu} = \frac{F_{pu} - F_{py}}{K_{p2}} + D_{py} \tag{22}$$

4.4. EEDP design process

The flowchart of the improved EEDP method for isolated HSR bridge is provided in Fig. 16, and the design steps are outlined as follows.

(1) Specify the design parameters of the HSR simply supported bridge, such as the mass m_1, stiffness K_{p1}, K_{p2} and the yield base shear F_{py} of the pier, and girder mass m_2.
(2) Select earthquake intensities and corresponding design response spectra, then select the type of isolation bearing and determine performance objectives (IO, SR and CP) at different earthquake intensities.
(3) Determine the relationship between the top displacement of isolated HSR bridge and the displacement of the ENLSDOF system by Equation (6).
(4) Calculate the fundamental period T of the ELSDOF system by Equation (10), and identify the yielding base shear F_y and yielding displacement d_y of the ELSDOF system on Fig. 13. Then calculate the sliding force F_{by} of the isolation bearing to target performance level of IO.
(5) Determine energy modification factor γ_a described in following section, and calculate the displacement d_p of the ENLSDOF system through Equation (17). Then obtain d_p, K_{eff} and D_{bp} through Equations (2) and (6) from the section 3, and calculate the sliding stiffness K_{b2} of the isolation bearing to target performance level of SR.
(6) Determine energy modification factor γ_b described in following section, and calculate the ultimate base shear F_u of ENLSDOF system through Equation (21). Then calculate the ultimate displacement D_{pu} of the pier at the MCE by Equation (22), and check whether the pier ductility factor is no larger than the value of 4.8 for performance level of CP.
(7) If the pier ductility factor is larger than the value of 4.8, return to step 4.
(8) If ductility factor of the pier meets the requirement, the seismic performance of the final designed structure should be evaluated via nonlinear dynamic analysis.

Table 3
Earthquake records.

No.	Name	Year	Magnitude	NGA#	Station
1	Chi-Chi Taiwan-05	1999	6.2	3160	TCU014N
2				3191	TCU081N
3	Imperial Valley-06	1979	6.53	175	E12140
4				167	CMP015
5	Northridge-01	1994	6.69	970	FAI095
6				1000	PIC090
7	Kobe_Japan	1995	6.9	1100	ABN000
8				1102	CHY000
9	Landers	1992	7.28	850	DSP000
10				3757	NPF090
11	San Fernando	1971	6.61	57	ORR021
12				83	PUD055
13	Loma Prieta	1989	6.9	762	FRE000
14				800	SJW160
15	Superstition Hills-01	1987	6.2	718	IVW090
16				726	WLF225

4.5. Modification factor γ_a

The energy modification factors in improved EEDP method are derived by nonlinear time history analysis of SDOF system. In this paper, A suite of 16 ground motions are selected from the PEER ground motion database [41], as listed in Table 3. These ground motions are selected based on the site classification II, the characteristic period zone is the 3rd type and the seismic fortification intensity is 8° according to GB50111-2006 [37]. The PGA corresponding to the SLE (63.2% probability of exceedance in 50 years), the DBE (10% probability of exceedance in 50 years) and the MCE (2% probability of exceedance in 50 years) are 0.1 g, 0.3 g and 0.57 g, respectively. Fig. 17 shows the design response spectra specified in GB50111-2006 [37], and spectra of the selected earthquake records scaled to DBE intensity.

In this section, the yield ratio η is defined as $\eta = F_p/F_y$, in which F_y and F_p are base shear of the ENLSDOF system at SLE intensity and DBE intensity, respectively. The yield ratio should satisfy the energy conservation and practical application requirements. Selecting a smaller yield ratio will result in a weaker structure. To dissipate the inputted seismic energy the structure would produce excessive displacement response; Selecting a larger yield ratio will result in a stronger structure that can withstand a strong earthquake without damages, but increase the material usage and lead to more economic investment. Therefore, choosing an appropriate yield ratio is crucial.

When the structural fundamental period T is determined, for a selected yield ratio, there are many possible values of γ_a. As shown in Fig. 18(a), any value can be set in the range of γ_a, and then if F_p is given, the corresponding displacement d_p of the ENLSDOF system can be obtained from Equation (17). The ENLSDOF system performs the time history analysis with the 16 selected earthquake records, and the mean value of the maximum displacement response of the ENLSDOF system at DBE intensity can be calculated. This value is compared with the determined displacement d_p given by Equation (17), and if the two values equal to each other, the trial value of γ_a can be seen as the correct modification factor. Fig. 18(b) shows the relationship between γ_a and

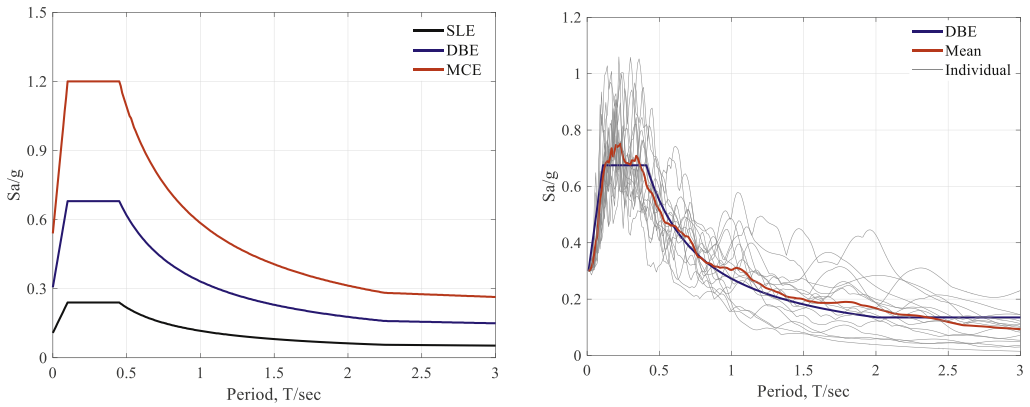

(a) Design response spectra (b) Earthquake records' spectra scaled to DBE level

Fig. 17. Response spectra of GB50111-2006 and earthquake records.

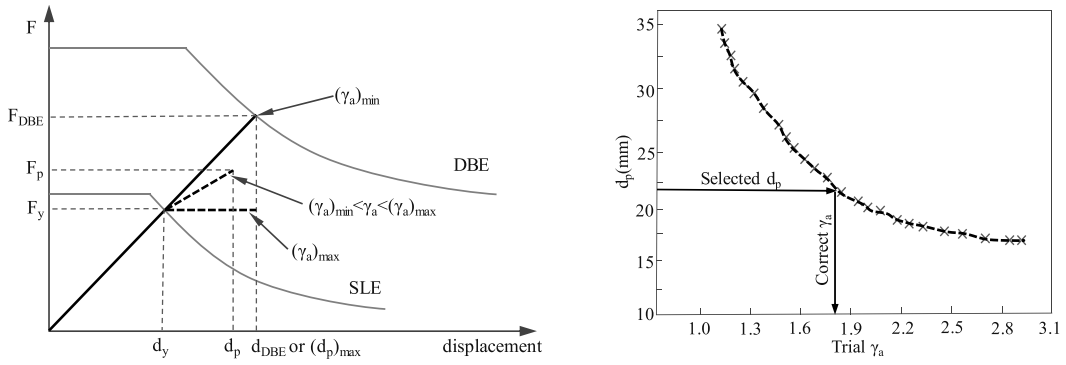

(a) Relationship between γ_a on d_p (b) Trial value of γ_a and selected d_p

Fig. 18. The calculation process for γ_a.

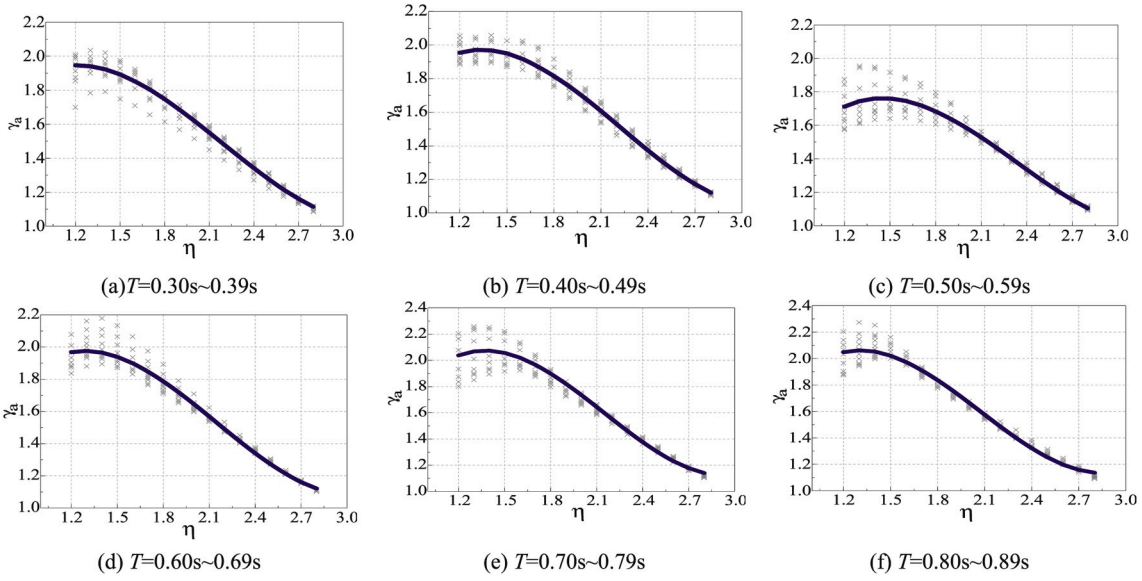

(a)T=0.30s~0.39s (b) T=0.40s~0.49s (c) T=0.50s~0.59s

(d) T=0.60s~0.69s (e) T=0.70s~0.79s (f) T=0.80s~0.89s

Fig. 19. Calculation values of γ_a and corresponding fitting cubic curves.

the displacement d_p of the ENLSDOF system at DBE intensity with T=0.39s and $\eta = 1.8$. Fig. 19 gives the calculation values of γ_a and corresponding fitting cubic curves. In this paper, γ_a are partitioned according to the period, and then, γ_a and η are fitted with the cubic curve as shown in Equation (23). The obtained corresponding coefficients of the fitting cubic curve are given in Table 4.

$$\gamma_a = p_1 + p_2\eta + p_3\eta^2 + p_4\eta^3 \tag{23}$$

Table 4
Coefficient values of the fitting cubic curves for γ_a

Period T	Coefficients			
	p_1	p_2	p_3	p_4
0.30~0.39	0.434	2.856	−1.628	0.248
0.40~0.49	−0.405	4.148	−2.216	0.332
0.50~0.59	−0.636	3.893	−1.947	0.278
0.60~0.69	−0.280	4.084	−2.263	0.351
0.70~0.79	−1.459	6.105	−3.268	0.507
0.80~0.89	−1.083	5.688	−3.178	0.511

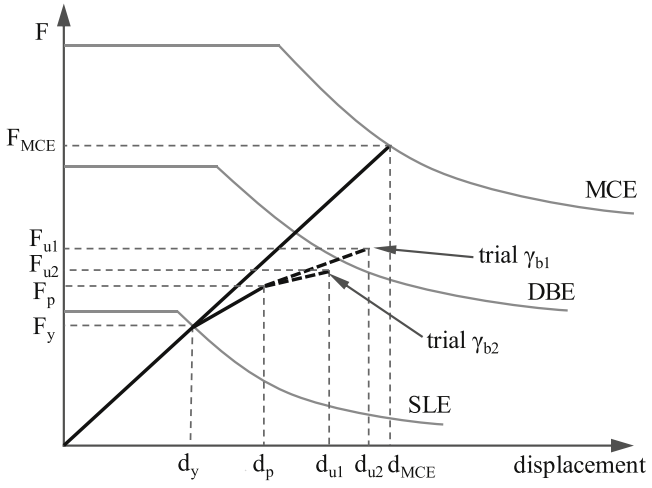

Fig. 20. The trial values of γ_b, F_u and d_u

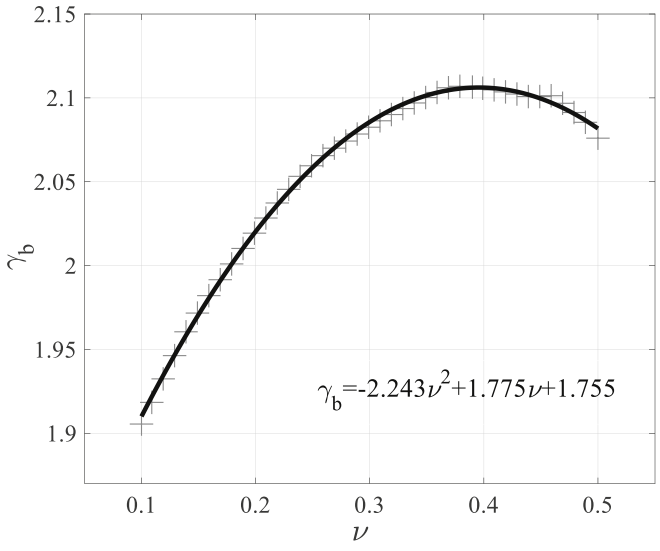

Fig. 21. The values of γ_b with T=0.831s, η = 1.9

4.6. Modification factor γ_b

To determine the complete trilinear behavior curve of the ENLSDOF system with known fundamental period T and yield ratio η, the definition of the post-yield stiffness ratio ν must also be introduced, that is, the ratio ν of the post-yield stiffness K_{py} to the post-yield ultimate stiffness K_{pu} of the ENLSDOF system, where $\nu = K_{py}/K_{pu}$. When the fundamental period T and yield ratio η of an ENLSDOF system are determined, the behavior curve of the ENLSDOF system can be obtained completely as long as the post-yield stiffness ratio ν is determined. Each post-yield

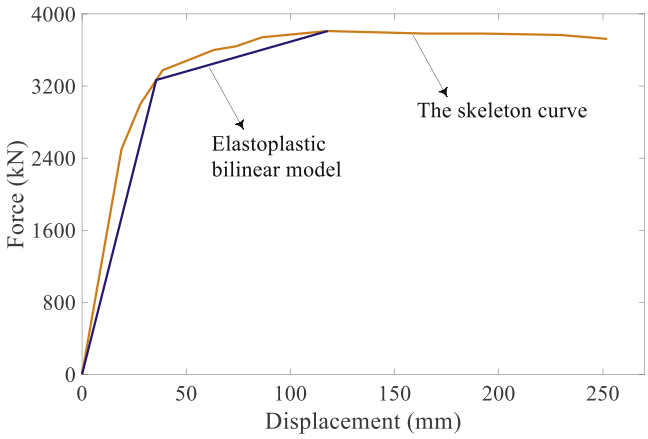

Fig. 22. The elastoplastic bilinear model of the SOL-2 prototype pier.

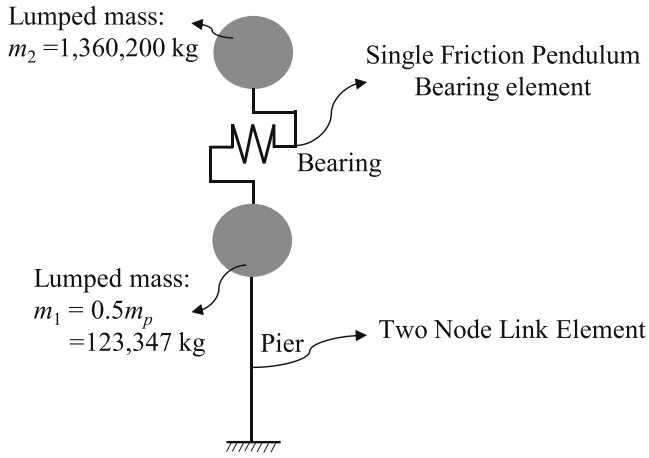

Fig. 23. The modeling approach of the finite element model based on OpenSee

stiffness ratio ν corresponds to the behavior curve of an ENLSDOF system. The ENLSDOF system performs the time history analysis with the 16 selected earthquake records, and the mean value of the maximum base shear and displacement of the ENLSDOF system at MCE intensity can be calculated. Substituting the mean value of the maximum base shear and displacement into Equation (21) gives γ_b corresponding to this ν, as shown in Fig. 20. Limited to space requirements, this paper only provides the values and fitting curve for γ_b in Fig. 21 with T=0.831s, η = 1.9, ν = 0.1~0.5.

5. Application of the proposed method for an isolated HSR bridge

To realize better seismic performance of isolated HSR bridge under different earthquake intensities, a FPB of the isolated HSR simply supported bridge in the longitudinal direction is designed by the proposed improved EEDP method, while the parameters of pier and girder are known. The SOL-2 pier specimen with the lowest longitudinal reinforcement ratio and axial load ratio of 8m pier in the experiment of Shao [18] is selected, the skeleton curve of the SOL-2 pier has been simplified into an elastoplastic bilinear model as shown in Fig. 22, in which the yield force F_{py} is 3266.47 kN, the corresponding displacement D_{py} is 35.59 mm, and the post-yield stiffness K_{p2} is 8194.642 kN/m. The girder and track component are considered as the lumped mass to characterize the inertial effects. To verify the effectiveness of the proposed improved EEDP method, the finite element model of the isolated HSR bridge is built by OpenSees, the modeling approach of the finite element model as

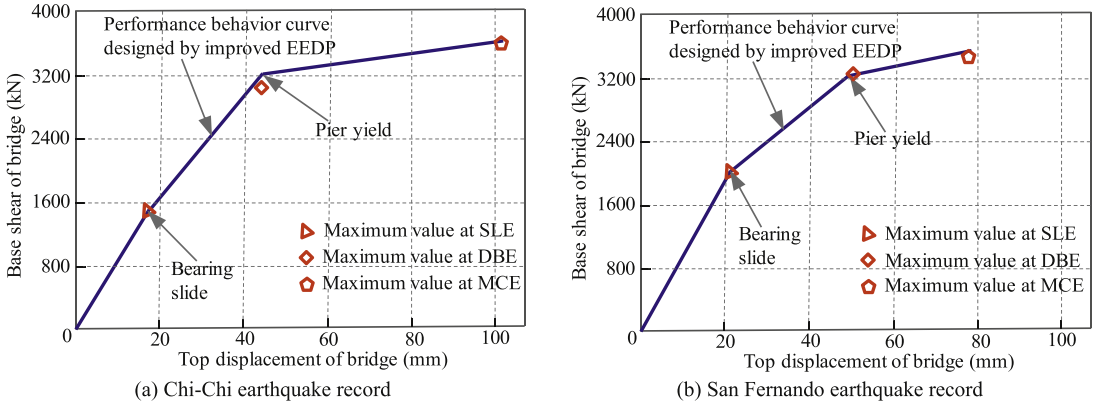

Fig. 24. Comparison of maximum value of time history analysis and results designed by the improved EEDP method.

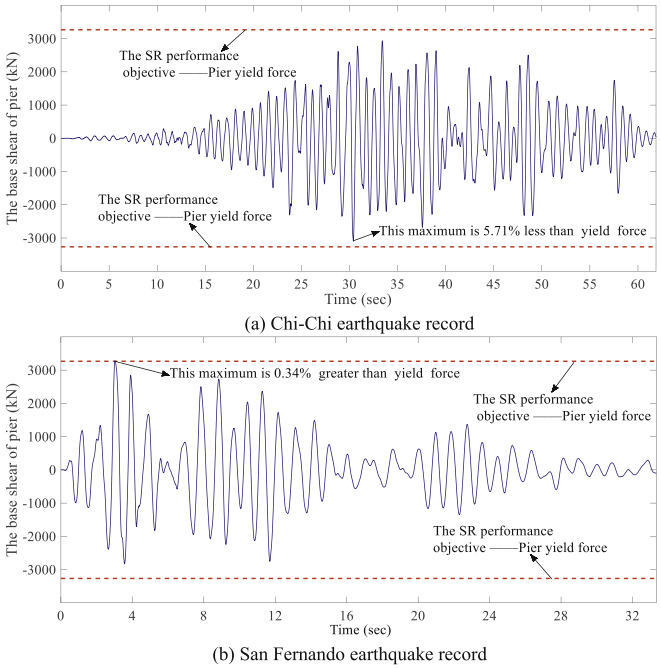

Fig. 25. Nonlinear time history responses of the pier's base shear at the DBE intensity.

shown in Fig. 23, and the seismic performance of the final designed isolated HSR bridge is evaluated via nonlinear dynamic analysis. The FPB is simulated using a special Single Friction Pendulum Bearing element, and the pier is simulated by a Two Node Link Element, and the horizontal behavior of the Two Node Link Element is simulated by Steel01 uniaxial material with the simplified elastoplastic bilinear model as shown in Fig. 22. In this paper, based on the individual seismic response spectra and the mean seismic response spectra of 16 earthquake records, the FPB of isolated HSR bridge are designed respectively.

5.1. Design based on the response spectra of individual earthquake record

In this section, two earthquake records (Chi-Chi and San Fernando) in Table 3 that match well with the design response spectra are selected, and are respectively scaled to SLE, DBE and MCE intensity for nonlinear time history analysis of the designed isolated HSR bridge with FPB. After the friction coefficient μ and sliding stiffness K_{b2} of the FPB are designed by the improved EEDP method, the finite element model is established for nonlinear time history analysis. Fig. 24 shows the comparison of maximum nonlinear time history analysis results and performance behavior curve designed by the improved EEDP method. Fig. 25 shows the nonlinear time history analysis responses of the pier's base shear at the DBE intensity by Chi-Chi and San Fernando earthquake records, respectively. Fig. 26 and Fig. 27 show the hysteretic curves from nonlinear time history analysis of the pier and bearing at different earthquake intensities by Chi-Chi and San Fernando earthquake records, respectively.

Fig. 24 shows that at the SLE intensity, the maximum values of nonlinear time history analysis responses for Chi-Chi and San Fernando earthquake records are nearly consistent with those designed by the improved EEDP method, and the FPB does not slide. It can be clearly seen from Fig. 26(a), (d) and Fig. 27(a), (d) that the FPB and the pier remain elastic through the hysteresis curve. In other words, the isolated HSR bridge designed by the EEDP method can achieve the expected IO performance objective. The maximum base shear of the pier from nonlinear time history analysis at the DBE intensity by Chi-Chi earthquake records is 5.71% less than the expected yield base shear, and the pier remains elastic as shown in Fig. 26(e). Meanwhile, the FPB is in the sliding state as shown in Fig. 26 (b). For San Fernando earthquake record, Fig. 25 (b) gives the error for the base shear of the pier is 0.34% and slightly greater than that for the expected yield base shear, while the top displacement of the model is slightly greater than the displacement designed by the improved EEDP method as shown in Fig. 24 (b). The pier has yielded and the FPB is in the sliding state as presented in Fig. 27(e) and 27 (b), respectively. The reason for the above errors is that many simplified calculations, such as equivalent linearization, are adopted in the design process, which leads to some errors. However, these errors are relatively small, and it can be considered that the improved EEDP method has basically achieved the expected SR performance objective at the DBE intensity. Fig. 26 (c), (f) and Fig. 27 (c), (f) indicate that the pier is in the yielding state, and the FPB is in the sliding state at the MCE intensity. The pier of the isolated HSR bridge meets the ductility requirements and do not collapse, so it achieves the expected CP performance objective by the improved EEDP method.

From the above results, when the same earthquake record is used for the isolated HSR bridge design and nonlinear time history analyses, the error for the maximum values from the nonlinear time history analysis and those calculated by the improved EEDP method were within 10% for the base shear and displacement of the isolated HSR bridges. The expected performance objectives of isolated HSR bridges at different earthquake intensities are nearly achieved, and it can be considered that the improved EEDP method has sufficient accuracy.

5.2. Design based on the mean response spectra of a suite of earthquake records

To verify the accuracy of the improved EEDP method and the equivalent SDOF system for practical engineering design, the mean

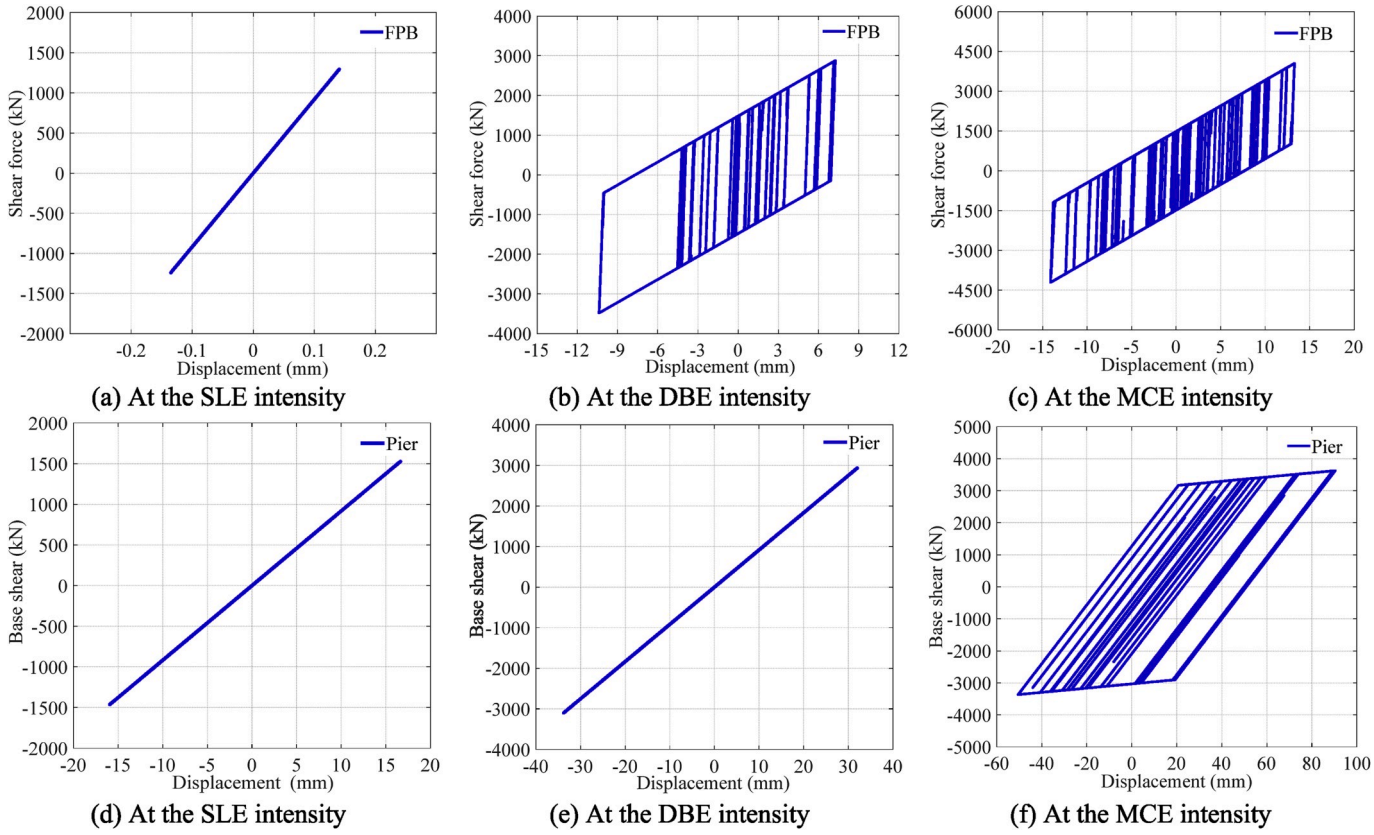

Fig. 26. Hysteresis curves with the Chi-Chi earthquake record.

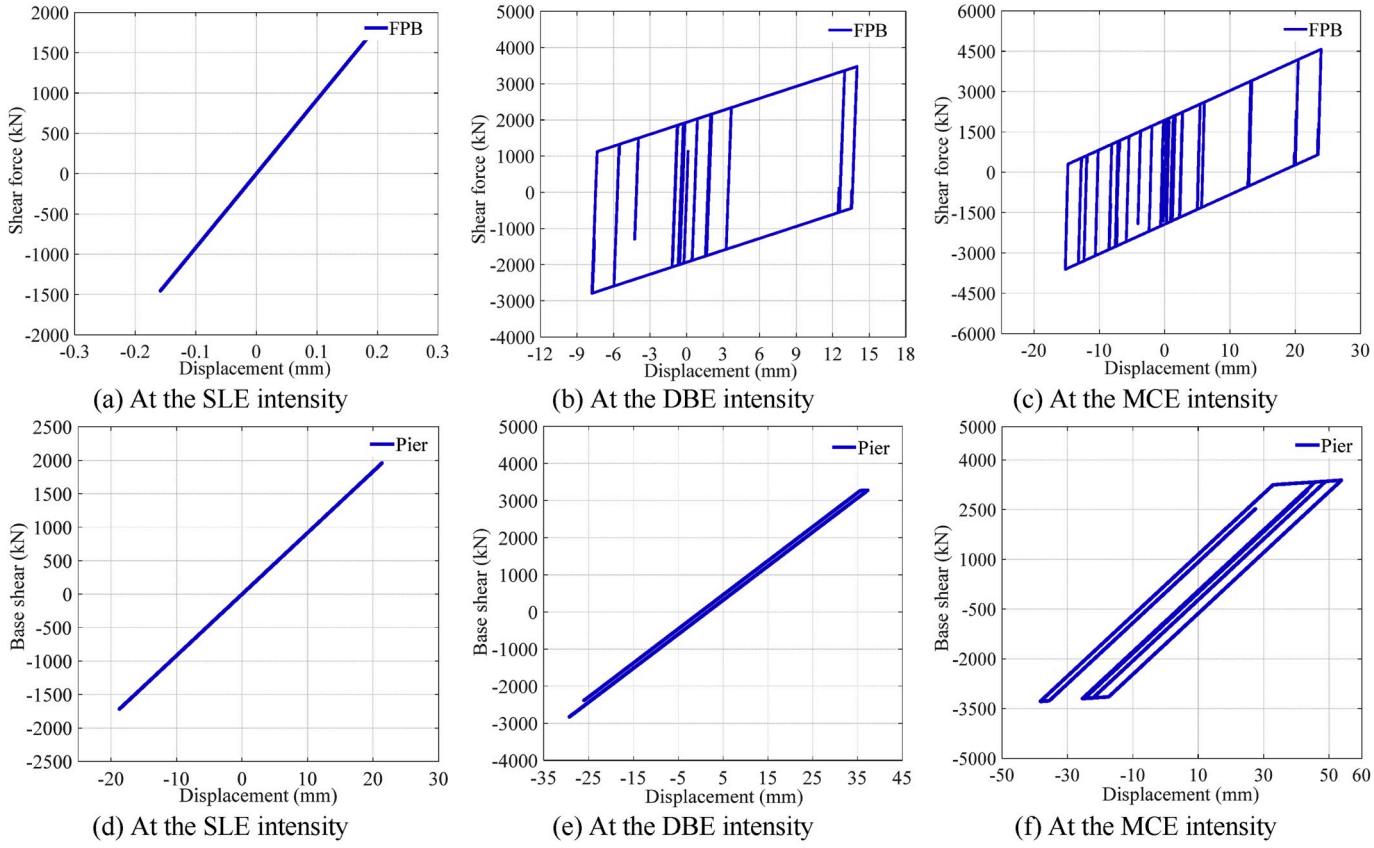

Fig. 27. Hysteresis curves with the San Fernando earthquake record.

Table 5
Design parameters for the isolated HSR bridge with FPB.

Parameters	Value	Remark
F_y	1721.41 KN	From Equation (10), Fig. 13
d_y	18.76 mm	From Equation (10), Fig. 13
D_y	18.76 mm	From Equation (13)
μ	0.109	From Equation (12)
γ_a	1.729	From Equation (23), Table 4
F_p	3266.47 KN	Defined
d_p	48.72 mm	From Equation (17)
D_p	50.40 mm	From Equation (6)
K_{b2}	91.75 KN/mm	From Equations (17) and (6), Fig. 11(a)
γ_b	1.937	From Fig. 21
F_u	3620.81 KN	From Equation (21)
D_u	105.42 mm	From Equation (6)

response spectra of 16 earthquake records mentioned in Table 3 was selected to complete the design the FPB of isolated HSR bridge. The parameters obtained by the improved EEDP method are shown in Table 5.

Fig. 28 (a) shows the performance behavior curve designed by improved EEDP method, a corresponding numerical analysis model of the isolated HSR bridge is established, and nonlinear time history analysis is performed by the 16 earthquake records listed in Table 3. The mean of maximum values of the base shear, the displacement of the pier and the displacement of the FPB calculated by the nonlinear time history analysis are compared with the values obtained by the improved EEDP method, as shown in Fig. 28 (b), (c), and (d).

At the SLE intensity, the results from the time history analysis are nearly consistent with those designed by the improved EEDP method as shown in Fig. 28, which means that the IO performance objective is achieved. At the DBE intensity, the mean base shear of the pier obtained by nonlinear time history analysis is 4.88% less than the expected yield base shear as indicated in Fig. 28 (b), and the pier did not yield. Meanwhile, the displacement of the pier is greater than the value designed by the improved EEDP method with 1.72% error as shown in Fig. 28 (c), and the displacement of the FPB is less than the value designed by the improved EEDP method with 0.87% error as shown in Fig. 28 (d). This basically meets the SR performance objective. At the MCE intensity, Fig. 28 (d) shows the displacement of the FPB is in good agreement with the expected design, and the base shear of the pier is 1.98% slightly less than the expected design value as shown in Fig. 28 (b), but the error for the displacement of the pier is 12.12% less than the value designed by the improved EEDP method as indicated in Fig. 28 (c). The pier of the isolated HSR bridge meets the ductility requirements and do not collapse, so the CP performance objective can be achieved. Based on the above analysis, the maximum error between the values of nonlinear time history analysis and the values designed by the improved EEDP method for the isolated HSR bridge is 12.12%, which proves that the improved EEDP method can better realize the performance design of isolated HSR bridges, and the calculation of the design process is simple and without complicated iterations.

6. Conclusions

Considering that HSR bridges could resist common earthquakes, however, collapse under stronger earthquakes. The isolation bearing can reduce the seismic damage and minimize the downtime of HSR simply supported bridges. To improve seismic performance of HSR bridges at different earthquake intensities, the FPB is adopted in this paper. Meanwhile, based on the analysis of experimental data, the improved performance objectives applicable to the isolated HSR bridges are proposed. To well design the isolated HSR bridges at different earthquake

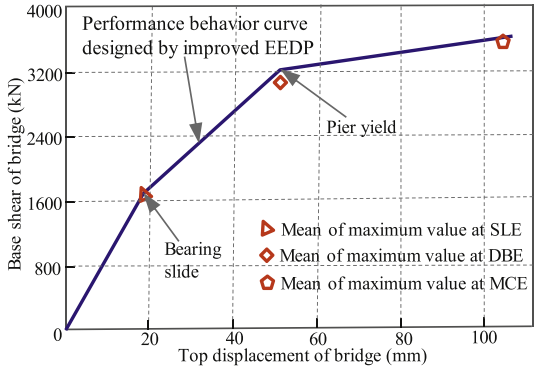

(a) Comparison of maximum value of time history analysis and results designed by the improved EEDP method

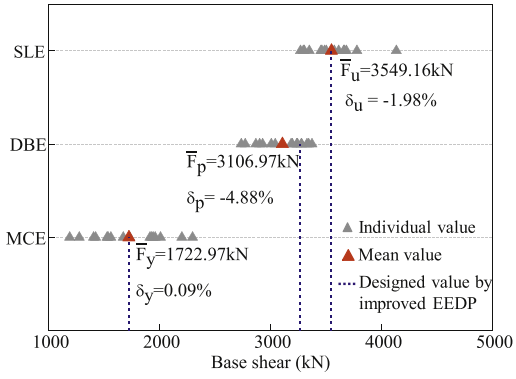

(b) The base shear of the pier

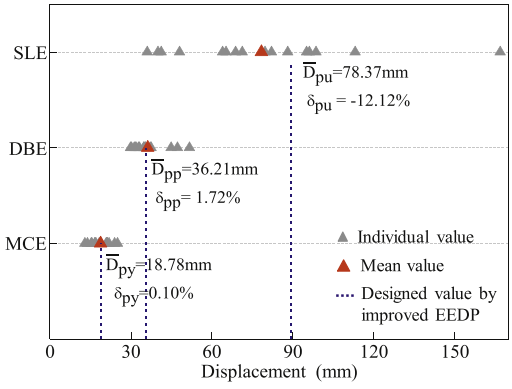

(c) The displacement of the pier

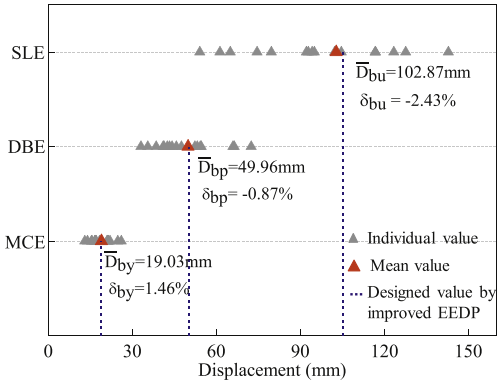

(d) The base shear of the FPB

Fig. 28. Comparison of the results of improved EEDP method and nonlinear time history analysis.

intensities, an effective design procedure is indispensable. This study presents an improved EEDP method, which considers multiple performance objectives, and takes the post-yield stiffness into account. The validity of the improved EEDP method is verified by numerical examples. The following conclusions are given:

(1) According to the analysis and calculation of the existing experimental data, it is found that the piers remain elastic during the SLE but yield during the DBE. Based on this, the improved performance objectives applicable to the isolated HSR bridges are proposed, which are IO, SR, and CP corresponding to SLE, DBE, and MCE intensity, respectively.
(2) The proposed design procedure is simple and can simultaneously achieve the three performance objectives at SLE, DBE and MCE intensity. The FPB of isolated HSR bridge is designed by the improved EEDP method, and the designed isolated HSR bridge realizes the trilinear force-deformation behavior and achieves the performance objectives of IO, SR, and CP without complicated iterations. Its effectiveness for designing the isolated HSR bridge has been proved.
(3) The results from the time history analysis are close to those designed by the improved EEDP method. The maximum error for the displacement of the pier is 12.12%, which proves that the improved EEDP method is sufficiently accurate.
(4) By adopting the FPB bearing instead of common bearing in HSR bridge, the seismic performance of HSR bridge is improved, and the pier is protected to avoid premature yielding at the DBE intensity. This proves that it is reasonable to adopt FPB in HSR bridge.
(5) The improved EEDP method proposed in this paper is currently only applied to simply supported bridges, and it should be extended to different bridge types and different structures in the future.

Declaration of competing interest

The authors declare that they have no known competing financial interests or personal relationships that could have appeared to influence the work reported in this paper.

CRediT authorship contribution statement

Wei Guo: Conceptualization, Methodology, Funding acquisition. **Qiaodan Du:** Data curation, Writing - original draft, Software. **Zhe Huang:** Data curation, Writing - original draft. **Hongye Gou:** Conceptualization, Methodology, Validation, Software, Supervision, Writing - original draft. **Xu Xie:** Writing - review & editing. **Yong Li:** Writing - review & editing.

Acknowledgement

This work was financially supported by the National Natural Science Foundation of China (51878674).

References

[1] He X, Wu T, Zou Y, Chen YF, Guo H, Yu Z. Recent developments of high-speed railway bridges in China[J]. Struct Infrastruct Eng 2017;13(12):1584–95. https://doi.org/10.1080/15732479.2017.1304429.
[2] Zheng J. Key technologies for high speed railway bridge construction[J]. Eng Sci 2008;10(7):18–27 (in Chinese).
[3] Li K, Guo Z, Wang L, Jiang H. Effect of seepage flow on shields number around a fixed and sagging pipeline[J]. Ocean Eng 2019;172:487–500. https://doi.org/10.1016/j.oceaneng.2018.12.033.
[4] Guo Z, Jeng DS, Zhao H, Guo W, Wang L. Effect of seepage flow on sediment incipient motion around a free spanning pipeline[J]. Coast Eng 2019;143:50–62. https://doi.org/10.1016/j.coastaleng.2018.10.012.
[5] Bi K, Hao H, Chen W. Effectiveness of using RFHDS connected PIP system for subsea pipeline vibration control[J]. Int J Struct Stabil Dynam 2018;18(8):1840005. https://doi.org/10.1142/S0219455418400059.
[6] Zhu Y, Wei YX. Characteristics of railway damage due to Wenchuan earthquake and countermeasure considerations of engineering seismic design[J]. Chin J Rock Mech Eng 2010;29(S1):3378–86 (in Chinese).
[7] Yan B, Dai GL, Hu N. Recent development of design and construction of short span high-speed railway bridges in China[J]. Eng Struct 2015;100:707–17. https://doi.org/10.1016/j.engstruct.2015.06.050.
[8] TB 10621-2009. Code for design of high speed railway[S]. Beijing, China: China railway publishing house; 2009.
[9] Guo W, Hu Y, Liu H, Bu D. Seismic performance evaluation of typical piers of China's high-speed railway bridge line using pushover analysis. Math Probl Eng 2019;2019:1–17. https://doi.org/10.1155/2019/9514769.
[10] Guo W, Zeng C, Gou H, Hu Y, Xu H, Guo L. Rotational friction damper's performance for controlling seismic response of high speed railway bridge-track system. Comput Model Eng Sci 2019;120:491–515. https://doi.org/10.32604/cmes.2019.06162.
[11] Chen L, Jiang L, Liu P. Seismic response analyses of high-speed railway bridge round-ended piers using global bridge model[J]. Int J Mater Prod Technol 2012;44(1/2):35. https://doi.org/10.1504/IJMPT.2012.048190.
[12] Guo W, Hu Y, Hou W, Gao X, Bu D, Xie X. Seismic damage mechanism of CRTS-II slab ballastless track structure on high-speed railway bridges[J]. Int J Struct Stabil Dynam 2019:2050011. https://doi.org/10.1142/S021945542050011X.
[13] Zhu Z, Wang L, Costa PA, Bai Y, Yu Z. An efficient approach for prediction of subway train-induced ground vibrations considering random track unevenness[J]. J Sound Vib 2019;455:359–79. https://doi.org/10.1016/j.jsv.2019.05.031.
[14] Zhu Z, Zhang L, Gong W, Wang L, Bai Y, Harik IE. An efficient hybrid method for dynamic interaction of train-track-bridge coupled system[J]. Can J Civ Eng 2019. https://doi.org/10.1139/cjce-2019-0020.
[15] Zhu Z, Gong W, Wang L, Li Q, Bai Y, Yu Z, Harik IE. An efficient multi-time-step method for train-track-bridge interaction[J]. Comput Struct 2018;196:36–48. https://doi.org/10.1016/j.compstruc.2017.11.004.
[16] Zhu Z, Gong W, Wang L, Bai Y, Yu Z, Zhang L. Efficient assessment of 3D train-track-bridge interaction combining multi-time-step method and moving track technique[J]. Eng Struct 2019;183:290–302. https://doi.org/10.1016/j.engstruct.2019.01.036.
[17] Jiang CW, Wei B, Wang DB, Jiang LZ, He XH. Seismic vulnerability evaluation of a three-span continuous beam railway bridge[J]. Math Probl Eng 2017;2017(4):1–13. https://doi.org/10.1155/2017/3468076.
[18] Shao GQ, Jiang LZ, Chouw N. Experimental investigations of the seismic performance of bridge piers with rounded rectangular cross-sections. J Earthquakes Struct 2014;7(25):463–84. https://doi.org/10.12989/eas.2014.7.4.463.
[19] Shrestha B, Hao H, Ibrahim NHJ, Bi K. On the effectiveness of rotational friction hinge damper to control responses of multi-span simply supported bridge to non-uniform ground motions[J]. Adv Struct Eng 2016;19(10):1575–91. https://doi.org/10.1177/1369433216645974.
[20] Yu Z, Li H, Wei B, Jiang L, Mao J. Numerical analysis on longitudinal seismic responses of high-speed railway bridges isolated by friction pendulum bearings[J]. J Vibroengineering 2018;20(4). https://doi.org/10.21595/jve.2017.18557.
[21] Tsopelas P, Constantinou MC, Kim YS, Okamoto S. Experimental study of FPS system in bridge seismic isolation[J]. Earthq Eng Struct Dynam 1996;25(1):65–78. https://doi.org/10.1002/(SICI)1096-9845(199601)25:1%3c65::AID-EQE536%3e3.0.CO;2-A.
[22] Kim YS, Yun CB. Seismic response characteristics of bridges using double concave friction pendulum bearings with trilinear behavior[J]. Eng Struct 2007;29(11):3082–93. https://doi.org/10.1016/j.engstruct.2007.02.009.
[23] Morgan TA, Mahin SA. Achieving reliable seismic performance enhancement using multi-stage friction pendulum isolators[J]. Earthq Eng Struct Dynam 2010;39(13):1443–61. https://doi.org/10.1002/eqe.1043.
[24] Fenz DM, Constantinou MC. Behaviour of the double concave friction pendulum bearing[J]. Earthq Eng Struct Dynam 2006;35(11):1403–24. https://doi.org/10.1002/eqe.589.
[25] Mosqueda G, Whittaker AS, Fenves GL. Characterization and modeling of friction pendulum bearings subjected to multiple components of excitation[J]. J Struct Eng 2004;130(3):433–42. https://doi.org/10.1061/(ASCE)0733-9445(2004)130:3(433).
[26] Ghobarah A. Performance-based design in earthquake engineering: state of development. J Eng Struct 2001;23(8):878–84. https://doi.org/10.1016/S0141-0296(01)00036-0.
[27] Calvi GM, Pavese A. Conceptual design of isolation systems for bridge structures [J]. J Earthq Eng 1997;1(1):193–218. https://doi.org/10.1080/13632469708962366.
[28] Jara M, Casas JR. A direct displacement-based method for the seismic design of bridges on bi-linear isolation devices[J]. Eng Struct 2006;28(6):869–79. https://doi.org/10.1016/j.engstruct.2005.10.016.
[29] Cardone D, Dolce M, Palermo G. Direct displacement-based design of seismically isolated bridges[J]. Bull Earthq Eng 2009;7(2):391–410. https://doi.org/10.1007/s10518-008-9069-2.
[30] Priestley MJN, Calvi GM, Kowalsky MJ. Direct displacement-based seismic design of structures[J]. J Earthq Eng 2005;9(2):257–78.
[31] Okuda M, Fukunaga S, Endo K. Seismic design and seismic performance retrofit study for the Akashi Kaikyo Bridge. J I Coast Archaeol 2009;5(2–3):109–18. https://doi.org/10.1080/15732480903142807.

[32] Li Y, Conte JP. Probabilistic performance-based optimum design of seismic isolation for a California high-speed rail prototype bridge[J]. Earthq Eng Struct Dynam 2018;47(2):497–514. https://doi.org/10.1002/eqe.2976.
[33] Goel SC, Chao SH. Performance-based plastic design: earthquake-resistant steel structures[M]. International Code Council; 2008.
[34] Goel SC, Liao WC, Reza Bayat M, Chao SH. Performance-based plastic design (PBPD) method for earthquake-resistant structures: an overview[J]. Struct Des Tall Special Build 2010;19(1-2):115–37. https://doi.org/10.1002/tal.547.
[35] Yang TY, Tung DP, Li Y. Equivalent energy design procedure for earthquake resilient fused structures[J]. Earthq Spectra 2018;34(2):795–815. https://doi.org/10.1193/122716EQS254M.
[36] Tung DP. Design and validation of innovative earthquake resilient fused structures [D]. University of British Columbia; 2017.
[37] GB50111-2006. Coad for seismic design of railway engineering[S]. Beijing, China: China planning press; 2009.
[38] Liu WF, Wang JT, Tang JW. Determining method of elasto-plastic double broken line model for seismic capacity curve[J]. Build Struct 2015.
[39] Housner GW. Limit design of structures to resist earthquakes[C]. In: Proceedings of the 1st 728 world conference on earthquake engineering. vol. 5; 1956. 1–5.13. 729.
[40] Uang C, Bertero VV. Use of energy as a design criterion in earthquake-resistant design[R]. Berkeley, California: College of Engineering; 1988. 730 Report No. UCB/EERC-88/18.
[41] PEER (Pacific Earthquake Engineering Research). Center strong motion database. University of California, Berkeley. http://peer.berkeley.edu/products/strong_ground_motion_db.html.